minerals

MDPI

Article

Single-Cell Imaging for Studies of Renal Uranium Transport and Intracellular Behavior

Shino Homma-Takeda [1,*], Hitomi Fujishiro [2], Izumi Tanaka [1], Haruko Yakumaru [1], Kyoko Ayama [1], Akihiro Uehara [1], Masakazu Oikawa [1], Seiichiro Himeno [2,3] and Hiroshi Ishihara [1]

[1] National Institute of Radiological Sciences, National Institutes for Quanum and Radiological Science and Technology, Chiba 263-8555, Japan; tanaka.izumi@qst.go.jp (I.T.); yakumaru.haruko@qst.go.jp (H.Y.); ayama.kyoko@qst.go.jp (K.A.); uehara.akihiro@qst.go.jp (A.U.); oikawa.masakazu@qst.go.jp (M.O.); ishihara.hiroshi@qst.go.jp (H.I.)

[2] Faculty of Pharmaceutical Sciences, Tokushima Bunri University, Tokushima 770-8514, Japan; donai-do@ph.bunri-u.ac.jp (H.F.); himenos@ph.bunri-u.ac.jp (S.H.)

[3] School of Pharmacy, Showa University, Tokyo 142-8555, Japan

* Correspondence: takeda.shino@qst.go.jp; Tel.: +81-43-382-5511

Abstract: Nephrotoxicity is the primary health effect of uranium exposure. However, the renal transport and intracellular behavior of uranium remains to be clearly elucidated. In the present study, the intracellular uranium distribution was examined with the cell lines derived from the S3 segment of mouse renal proximal tubules, which is a toxic target site of uranium, using microbeam-based elemental analysis. Uranium exposure at 100 μM for 24 h (non-toxic phase) was performed in S3 cells. Two types of measurement specimens, including those that are adhesive cell specimens and cryosection specimens, were examined for the positional relationship of the intracellular localization of uranium. Based on the combined results of single-cell imaging from the two types of cell specimens, uranium was distributed inside the cell and localized in the cytoplasm near the cell nucleus. In some cells, uranium was colocalized with phosphorus and potassium. The amount of uranium accumulated in S3 cells was estimated using thin section-standards. The mean uranium content of three adhesive cells was hundreds of femtogram per cell. Thus, we believe that single-cell imaging would be useful for studies on renal uranium transportation and cellular behavior.

Keywords: uranium; imaging; proximal tubules; S3 segments; distribution; PIXE

Citation: Homma-Takeda, S.; Fujishiro, H.; Tanaka, I.; Yakumaru, H.; Ayama, K.; Uehara, A.; Oikawa, M.; Himeno, S.; Ishihara, H. Single-Cell Imaging for Studies of Renal Uranium Transport and Intracellular Behavior. *Minerals* **2021**, *11*, 191. https://doi.org/10.3390/min11020191

Academic Editor: Daniele Moro

Received: 30 December 2020
Accepted: 10 February 2021
Published: 12 February 2021

1. Introduction

Uranium is a naturally occurring radioactive heavy metal. It is a component of the earth's crust and is widely present in natural environments, such as soil and water, as well as in foods. The daily intake of uranium is approximately 1 μg per person [1]. This value is one-fourth and one-twentieth of those of toxic heavy metals, such as mercury and cadmium, respectively [2,3]. The drinking water guideline specified by the World Health Organization (WHO) for uranium is 30 μg/L [4]. In addition, the uranium levels in surface and groundwater are generally as low as the sub ppb [5]. However, it is known that the chronic ingestion of uranium at higher levels via contaminated groundwater results in an induction of renal damage [6,7]. Moreover, uranium is used as a fuel in nuclear power plants. The recent nuclear accident in Japan, following the earthquake and tsunami in 2011, has led to increasing public concern regarding the health effects of uranium.

The kidney and bone are the main sites of deposition of uranium after uranium ingestion [8,9]. Uranium is known to exhibit chemical and radiological toxicities and cause tissue damage to the kidney. Uranium is an α-particle radionuclide. Alterations in solute transport and induction of oxidative stress have been reported in terms of chemical toxicity of uranium, even though the details of these mechanisms have not been clearly understood [10,11]. Uranium-induced renal toxicity is characterized by a tubular damage of the

downstream region of the proximal tubules (S3 segments of the proximal tubule) [12,13], which leads to the failure of tubular reabsorption [6,7] as well as proteinuria [14]. We demonstrated the site-specificity of uranium accumulation [15,16] and formation of uranium concentration using microbeam-based elemental analysis in micro-regions [17] in the S3 segments of the proximal tubule of rat kidneys during acute renal toxicity. The uranium-concentrated areas were still detected during recovery [17]. Uranium in these areas was partially reduced [18]. In addition, phosphorus and potassium were colocalized in some of these areas [19]. The formation mechanism of uranium bioconcentration is a key determinant of uranium toxicity because the remaining uranium can cause future deleterious effects. Intracellular uranium dynamics research, including the involvement of biomineralization, is required.

The renal proximal tubules play pivotal roles in the reabsorption of substances from the glomerulus-filtered urine. It is divided into three regions from the upstream, which include S1, S2, and S3 segments with region-specific material transport systems. Cell lines derived from the tubular region [20–22] are useful for studies regarding the tubular transport of nephrotoxic metals. The gene expression of metal transporters and antioxidant enzymes differ in these segments [23]. The mechanism of segment-specific cadmium absorption and excretion has been clarified [24,25]. Microbeam scanning elemental analysis, which is also known as μ-PIXE (particle-induced X-ray emission with microprobe) analysis, is one of the suitable analytical techniques for detecting the precise distribution of elements in a small specimen with good detection of light elements, such as phosphorus, potassium, and calcium. Our previous studies with animal experiments suggested the co-localization of uranium and the light elements in the renal tubules [19] albeit the positional relationship of these elements in the cell remains unclear. PIXE imaging of S3 cells may provide new insights into the implications of cellular uranium dynamics.

In the present study, single-cell elemental imaging was performed using S3 cells derived from mouse renal proximal tubules by μ-PIXE analysis. In addition to the specimens of adhesive cells, cryosection specimens of S3 cells were also subjected to μ-PIXE to confirm the transfer of uranium into cells.

2. Materials and Methods

2.1. Chemicals

Uranyl acetate (depleted uranium) was obtained from Wako Pure Chemical Industries Ltd. (Osaka, Japan), and the optimal cutting temperature (OCT) compound was obtained from Sakura FineTechnical Co. Ltd. (Tokyo, Japan). Nitric acid (ultrapure analytical reagent) was obtained from Tama Chemicals (Kawasaki, Japan), whereas poly-L-lysine hydrochloride (Mw > 12,000) was obtained from Peptide Institute Incorporation (Osaka, Japan).

2.2. Cell Culture and Uranium Treatment

Details of the establishment of the immortalized S3 cells from mouse proximal tubules have been previously described [20–22]. S3 cells were cultured in Dulbecco's modified Eagle's medium/Ham's Nutrient Mixture F12 supplemented with 5% fetal bovine serum (FBS), 1 μg/mL insulin, 10 ng/mL epidermal growth factor, 10 μg/mL transferrin, 100 unit/mL penicillin, and 100 μg/mL streptomycin under 5% CO_2 at 37 °C.

Uranyl acetate was dissolved in filtered double distilled water to obtain the stock solution containing 20 mM as U and 200 mM $NaHCO_3$. The stock solution was diluted with the cell culture medium and cells were incubated with the medium containing uranium. Control cells were incubated with the medium without uranium.

2.3. Cytotoxicity Studies

Cells were seeded onto 96-well microplates (2×10^4/well) and incubated for 24 h, and then treated with uranium (0.1–600 μM) for 24 h. Sensitivity to uranium was measured

by colorimetry using the alamarBlue (Biosource International, Camarillo, CA, USA), as described previously [26].

2.4. Specimen Preparation for Uranium Imaging

2.4.1. Experiment 1: Adhesive Cells

Polypropylene film (3 cm × 3 cm, 6-µm thick) was attached to culture dishes (diameter of 6 cm), and these dishes were incubated with double distilled water for 1 h, which was followed by incubation with 100% ethanol for 1 min. A surface of the polypropylene film was immersed in 90% ethanol solution of 0.1 mg/mL poly-L-lysine. After drying, the dishes were further incubated with culture medium for 24 h at 37 °C. 3×10^5 cells were seeded onto the dishes and incubated for 24 h, and then the medium was replaced with uranium-containing medium. After 24 h of incubation, cells were washed with phosphate buffered saline (PBS), fixed in cold methanol for 10 min (−20 °C), and dried. Cells attached to the polypropylene films were placed on sample holders for PIXE analysis.

2.4.2. Experiment 2: Cryosections of Cells

Unlike the above experiment, normal culture dishes (diameter, 6 cm) were used in the following experiments. 3×10^5 cells were seeded onto the dishes, incubated for 24 h, and the medium was replaced with uranium-containing medium. After 24 h of incubation, cells were washed with PBS and collected. The experiment was performed in quadruplicate. Three dishes were used for measuring uranium concentration in cells (uranium uptake experiment). The remaining one dish was used for cryosection specimens. The cells were embedded in the OCT compound and frozen with liquid nitrogen. Then frozen cells were sectioned to a thickness of 2 µm using a cryomicrotome. The slices were placed on polypropylene films and subjected to PIXE analysis. The experimental design is shown in Figure 1.

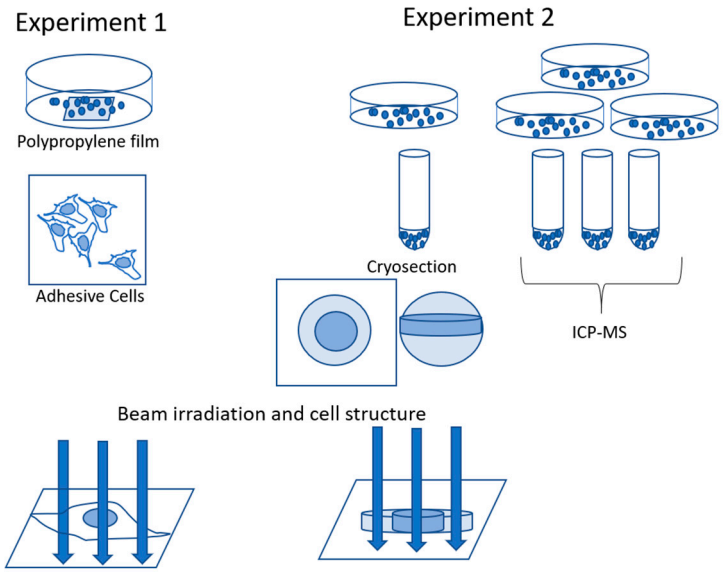

Figure 1. Experimental design.

2.5. Uranium Uptake Experiment

The estimation of uranium uptake into the S3 cells was performed using collected cell specimens. The collected cells ($103 \pm 18 \times 10^6$ cells) were digested with ultrapure nitric acid under microwave heating. Each specimen was diluted with ultrapure water, and uranium concentrations were determined by using inductively coupled plasma-mass spectrometry (ICP-MS, Agilent 7500a, Yokogawa Analytical Systems, Inc., Tokyo, Japan). The calibration curves were derived by using standard solutions on the SPEX Multi-element Plasma Standard (SPEX CertiPrep Group L.L.C., Metuchen, NJ, USA). The recovery rate

was 103 ± 3%, and the detection limit of uranium was 0.015 ng g^{-1} under our experimental conditions. The bulk value was calculated by dividing the amount of uranium in the collected cells by the number of cells.

2.6. μ-PIXE Analysis

Cellular imaging of uranium and endogenous elements was performed using a Model OM-2000 microbeam scanning PIXE system (Oxford Microbeams Ltd., Oxford, UK) with a Si (Li) detector for light elements and a CdTe detector for uranium [27]. Elemental images were constructed using the intensity data of the P Kα, S Kα, Cl Kα, K Kα, and U Lβ1 lines at each point, which were obtained by scanning the specimens under the following conditions: proton energy, 3.0 MeV, integrated charge, 0.2 μC, and spatial resolution, 1 μm × 1 μm. The Lβ1 line was used for uranium imaging and quantitative validation because endogenous renal rubidium [28] interferes with the detection of the uranium Lα line. Quantitative validation of uranium in cells of adhesive cell specimens and cryosection specimens was performed using thin-section standards of uranium for the microbeam analysis (2 μm) [29]. A calibration line was obtained from the mean total intensity of U Lβ1 (17.15–17.43 keV) in 20 μm × 20 μm areas in each standard section.

3. Results

3.1. Sensitivity of S3 Cells to Uranium

Exposure of S3 cells to uranium for 24 h did not result in a significant increase in mortality up to 600 μM (Figure 2), even though higher doses caused toxic effects after several days of exposure in our preliminary experiments. In the present study, further experiments were performed under the exposure condition of 100 μM.

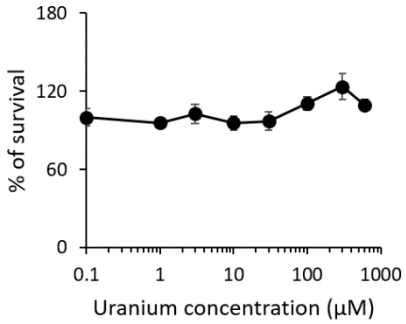

Figure 2. Uranium cytotoxicity in S3 cells.

Cells were exposed to uranium for 24 h. Cell cytotoxicity was quantified using the alamarBlue assay. The uranium concentrations are presented on the logarithmic scale with base 10. Each point is expressed as the mean ± SD from quintuple.

3.2. Elemental Imaging of S3 Adhesive Cells (Experiment 1)

An example of the X-ray spectrum from control and uranium-treated S3 cells is depicted in Figure 3. Chlorine, sulfur, phosphorus, and potassium were detected in both the control and uranium-treated S3 cells (Figure 3, left panel). Clear peaks of calcium were not detected in these S3 cells under the condition of a 0.2-μC integrated charge. The uranium spectrum was confirmed in the uranium-treated S3 cells (Figure 3, right panel). Clear images were obtained for chlorine, sulfur, phosphorus, and potassium in the control S3 cell (Figure 4). Chlorine was distributed throughout the cell. Phosphorus, sulfur, and potassium were distributed in the area closer to the center of the cell, where the nucleus is located than the chloride distribution.

After uranium exposure, phosphorus and potassium localization was observed in some cells (Figure 5, upper panel). Uranium was colocalized with phosphorus and potassium. The colocalization was found in the region near the edge of the cell (Figure 5, upper

and middle arrows), even though the localization was also found in the region near the center of the cell (Figure 5, upper and lower arrows). Elemental images with higher resolution indicated that uranium colocalized with phosphorus and potassium was found slightly off the position of the cell nucleus in the center of the cell (Figure 5, Lower panel). To clarify whether uranium was localized on the cell surface or inside the cell, cryosections of S3 cells exposed to uranium were subjected to imaging analysis.

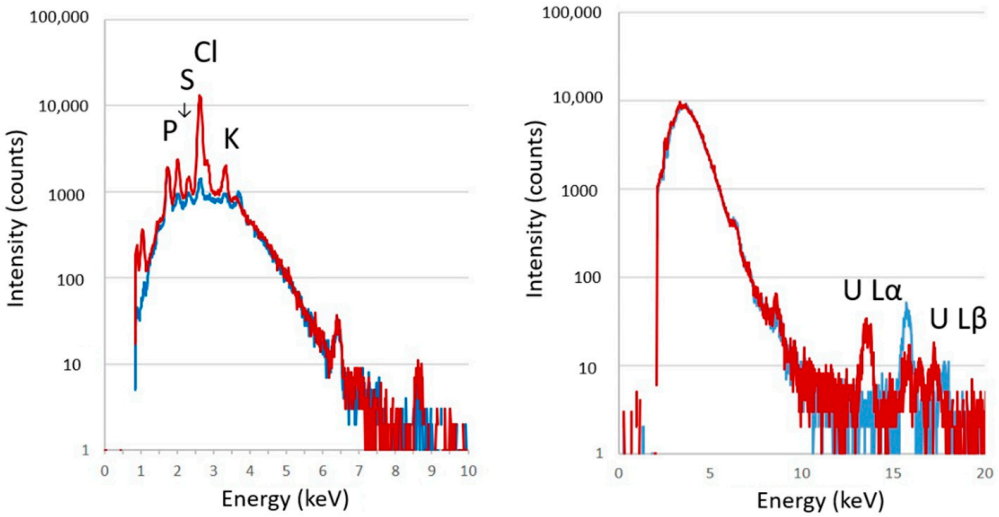

Figure 3. PIXE spectra of S3 cells obtained by scanning at areas in Figures 4 and 5. Blue line, control. Red line, uranium-treated. Scanning area, 50 μm × 50 μm. Integrated charge, 0.2 μC. Beam size of 1 μm × 1 μm with the Si (Li) detector (**left**) and CdTe detector (**right**).

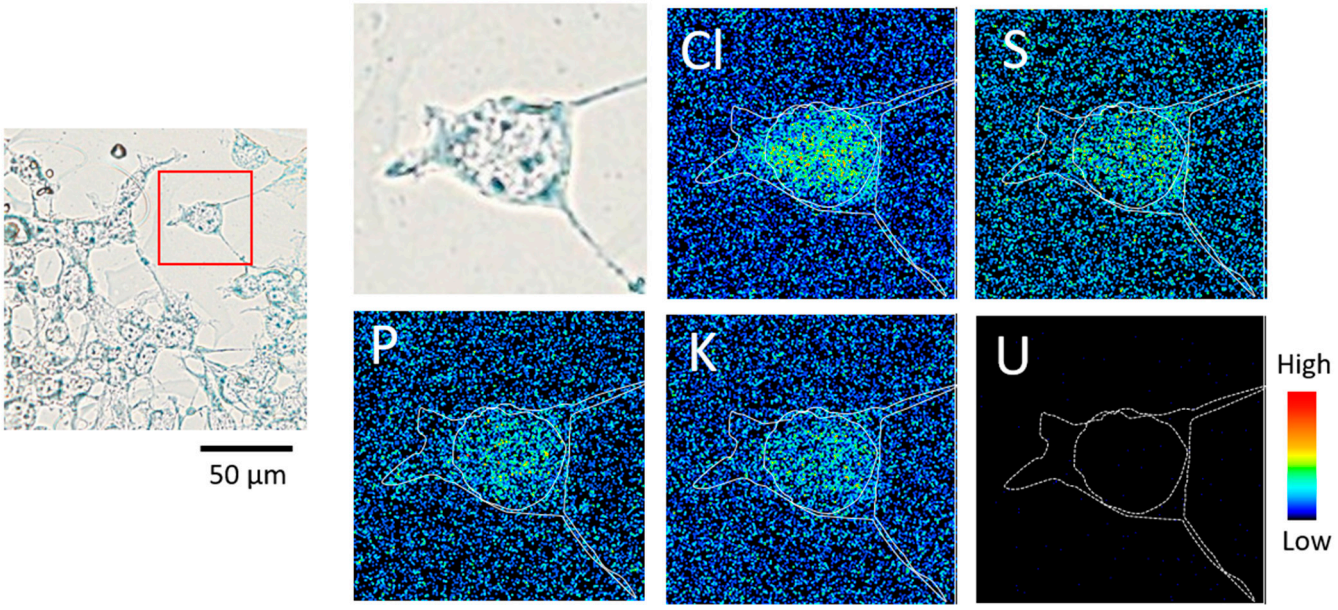

Figure 4. PIXE imaging of control S3 cells. (**Left panel**) Photo of control S3 cells. Elemental imaging was performed with the following conditions in the boxed area. Scanning area, 50 μm × 50 μm. Integrated charge, 0.2 μC, and beam size of 1 μm × 1 μm.

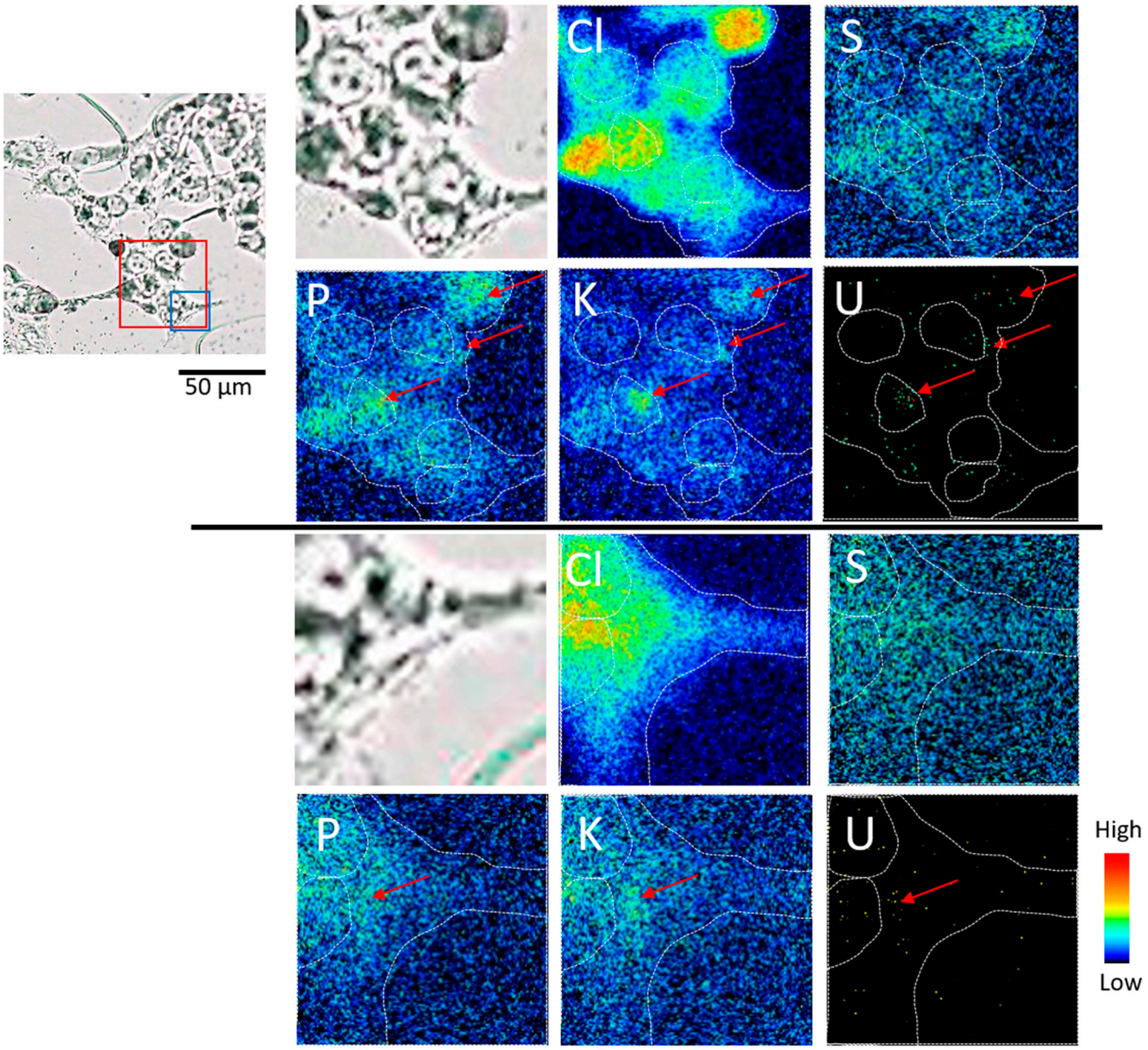

Figure 5. PIXE imaging of uranium-treated S3 cells. (**Left panel**) Photo of S3 cells exposed to uranium for 24 h. Elemental imaging was performed with the following conditions in the boxed areas: scanning area, 50 µm × 50 µm (red), 25 µm × 25 µm (blue), integrated charge, 0.2 µC, and beam size, 1 µm × 1 µm (**Upper panel**). Elemental images are in the red boxed area (**Lower panel**). Elemental images are in the blue boxed area. Arrows indicate colocalization of phosphorus, potassium, and uranium.

3.3. Elemental Imaging of Cryosections of S3 Cells (Experiment 2)

The distribution of phosphorus also corresponded to the cell nucleus in cryosection specimens (Figure 6). Uranium was detected inside S3 cells, and the distribution of uranium was slightly outside the distribution of phosphorus (Figure 6, dashed line), indicating that uranium was distributed in the cytoplasm near the cell nucleus. Cells colocalized with uranium and potassium were also observed.

3.4. Amount of Uranium Accumulated in Cells

The amount of uranium accumulated in S3 cells after 24-h treatment of uranium was estimated using thin section standards. The mean uranium content of three adhesive cells was 398 ± 280 fg per cell. The mean uranium concentration of the four cell cryosection

specimens examined was 335 ± 190 μg/g. It was equivalent to 766 ± 436 fg per cell, assuming a sphere with a cell diameter of 18 μm. Since the uranium localization region was unevenly distributed in the cell, it can be considered that the uranium level differs depending on the cryosection. The differences in the cell state, such as the cell cycle condition, may also be one of the factors influencing the variation. The bulk value from the Uranium Uptake Experiment using ICP-MS was found to be 137 ± 49 fg per cell.

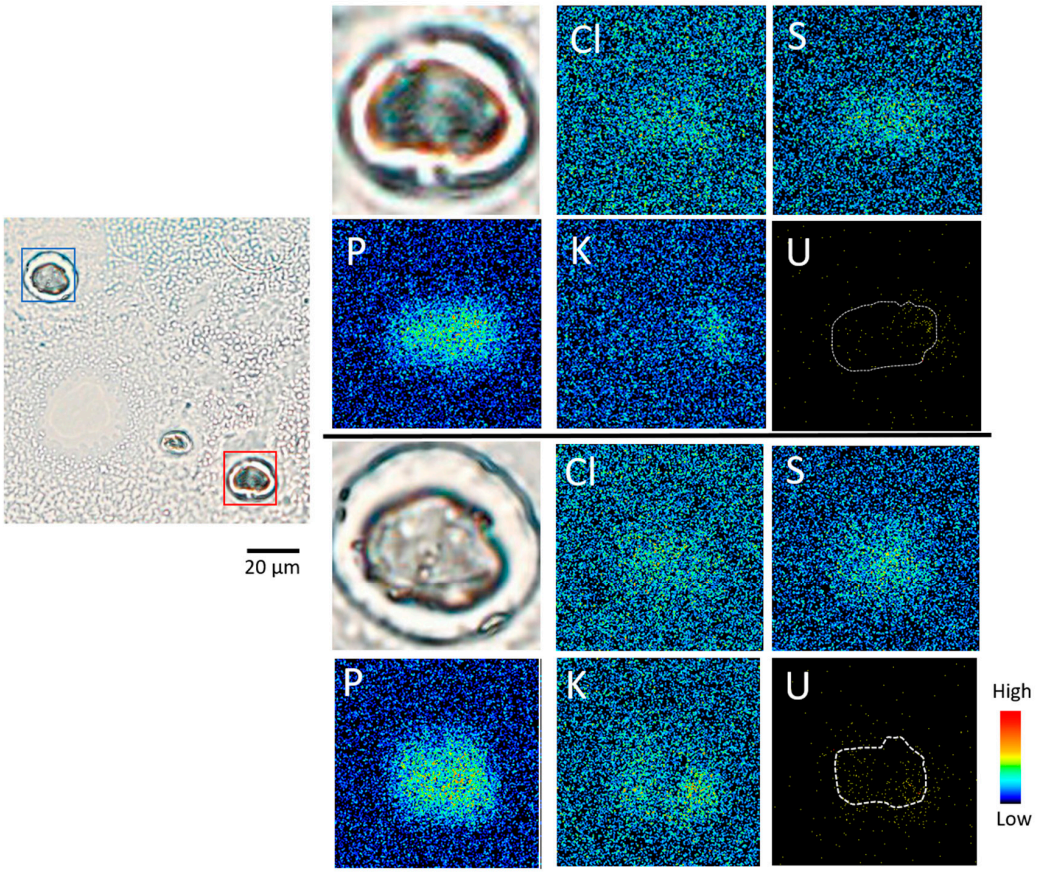

Figure 6. PIXE imaging of cryo-section of uranium-treated S3 cells. (**Left panel**) Photo of cryosection of S3 cells exposed to uranium for 24 h. Elemental imaging was performed with the following conditions in the boxed areas: scanning area, 20 μm × 20 μm, integrated charge, 0.2 μC, and beam size, 1 μm ×1 μm (**Upper panel**). Elemental images are in the red boxed area (**Lower panel**). Elemental images are in the blue boxed area. Dashed line corresponds to phosphorus distribution.

4. Discussion

Single-cell elemental imaging using cell lines could be performed using sample supports of special materials, such as a silicon nitride membrane [30]. A versatile, thin membrane, such as a polycarbonate membrane, has been used in the other studies [31,32], but the size of the container for culturing cells in these studies was very small (several to dozen of mm^2) compared with the cell culture dishes for general metal uptake or gene expression experiments. The present method was designed to obtain information regarding elemental imaging in a series of nephrotoxicological experiments. Hence, general-purpose cell dishes with an attached membrane were used. This enabled the comparison of information from a single cell with the values of the bulk experiments.

The type of adhesive cell specimens has the advantage of closely resembling a living state. However, the data obtained is the total elemental information of different cell structures in the region of the central part of the cell (Figure 1). Even if uranium is attached to the cell surface, it appears as if it is localized inside the cell. Therefore, a type of cryosection specimen was examined by image analysis to solve this problem. Combining

the results of the adhesive type and the section type, it was demonstrated that uranium was distributed inside the cell and localized in the cytoplasm near the cell nucleus. In some cells, uranium was colocalized with phosphorus and potassium. Calcium localization was not observed in the areas of uranium localization under the uranium exposure condition of 100 μM for 24 h. From the two types of cell imaging, it was suspected that sulfur was abundantly distributed in the nucleus, and chlorine was also abundant in the cell surface.

The intracellular dynamics of uranium agreed with the results of rat experiments, where highly concentrated uranium with 50-fold above the mean renal uranium concentration was observed near the nuclei of the S3 segments of the proximal tubule at the early phase of toxicity [17]. In addition, uranium detection has been reported in the perinuclear regions with nerve-derived cells [32], while uranium nuclear translocation in the early phase of exposure has been demonstrated with the liver and kidney cells [33,34]. Uranium colocalization with phosphorus and potassium was observed at the early stages of toxicity, even though uranium compounds precipitate in the cytoplasmic compartment in the form of uranyl phosphate needles after exposure to toxic concentrations (400–2000 μM) of uranium [35–37]. The reason for potassium and uranium colocalization cannot be clearly explained, but it has also been confirmed using in vivo systems in uranium-treated rat renal tubules [19]. Protein aggregation due to uranium-protein interaction may also be a reason for detection at the early phase of toxicity because uranyl ions have a high affinity for phosphate groups on biomolecules [38–40], even though the formation mechanism is not well understood. In addition to S3 cells, experiments with other types of cells, such as S1 and S2 cells, would provide insights for understanding the characteristics of intracellular uranium dynamics of S3 cells and may lead to the elucidation of the mechanism of uranium localization. Persistent accumulation of uranium may have long-term effects, considering that uranium is an α-particle radionuclide. Further experiments are required to investigate how the elements accumulate over time and whether the accumulation associated with biomineralization was not recognized at the early phase of toxicity, despite the colocalization of calcium in uranium-concentrated areas.

5. Conclusions

The intracellular uranium distribution was examined with cultured S3 cells derived from mouse renal proximal tubules by μ-PIXE analysis. Using two types of measurement specimens (adhesive cell specimens and cryosection specimens), the positional relationship of the intracellular localization of uranium was obtained in detail. Uranium was distributed inside the cell and localized near the cell nucleus. The quantitative validation of single-cell imaging of uranium was also performed. This experimental method would be useful for studies on uranium renal transport and cellular behavior.

Author Contributions: Conceptualization, S.H.-T. and H.F. Methodology, S.H.-T., H.F., and M.O. Validation, S.H.-T., H.F., and M.O. Formal analysis, S.H.-T., H.F. and M.O. Investigation, S.H.-T., H.F., I.T., K.A., A.U. and H.I. Resources, S.H.-T., H.F., I.T. and H.I. Data curation, S.H.-T., H.F., H.Y. and M.O. Writing—original draft preparation, S.H.-T. Writing—review and editing, S.H.-T., H.F., H.Y., A.U., S.H. and H.I. Visualization, S.H.-T. and H.Y. Supervision, S.H.-T. Project administration, S.H.-T. and S.H. Funding acquisition, S.H.-T. All authors have read and agreed to the published version of the manuscript.

Funding: This work was partially supported by a Grant-in-Aid for Scientific Research (19H05775) from the Japan Society for the Promotion of Science.

Acknowledgments: PIXE experiments proceeded at the Electrostatic Accelerator Facilities in National Institute of Radiological Sciences, National Institutes for Quantum and Radiological Science and Technology under the auspices of a research project with NIRS-Sharing of advanced research infrastructure (Proposal No. 20P JO9). We thank Yuuki Uematsu of the Department of Engineering and Safety, Yoshinari Shiino and Tsuyoshi Hamano of the Department of Research Planning and Promotion, National Institute of Radiological Sciences, for their assistance with experimental procedures involving nuclear fuel materials, and Hiroyuki Iso, Takuya Matsuda, and Yuichi Higuchi of the National Institute of Radiological Sciences, for their technical support during PIXE measurements,

and Teruaki Konishi of Institute for Quantum Life Science, National Institutes for Quantum and Radiological Science and Technology for constructive advices for the preparation of adhesive cell specimens. We also thank Hiroshi Yoshida of Tokyo Nuclear Services Co., Ltd., for monitoring contamination during the study.

Conflicts of Interest: The authors have no conflicts of interest to declare.

References

1. Shiraishi, K.; Tagami, K.; Muramastu, Y.; Yamamoto, M. Contributions of 18 food categories to intakes of 232Th and 238U in Japan. *Health Phys.* **2000**, *78*, 28–36. [CrossRef] [PubMed]
2. World Health Organization. *IPCS Assessing Human Health Risks of Chemicals: Derivation of Guidance Values for Health-Based Exposure Limits*; International Programme on Chemical Safety: Geneva, Switzerland, 1994.
3. Food Safety Committee. *Document on Safety of Dietary Cadmium Intake*; Minster of Health, Labour and Welfare of Japan: Tokyo, Japan, 2008.
4. WHO. *Guidelines for Drinking-Water Quality*; WHO: Geneva, Switzerland, 2011; Volume 1, pp. 430–431, 475.
5. Uchida, S.T.K.; Tabei, K.; Hirai, I. Concentrations of REEs, Th and U in river waters collected in Japan. *J. Alloy. Compd.* **2006**, *408/412*, 525–528. [CrossRef]
6. Kurttio, P.; Auvinen, A.; Salonen, L.; Saha, H.; Pekkanen, J.; Mäkeläinen, I.; Väisänen, S.B.; Penttilä, I.M.; Komulainen, H. Renal effects of uranium in drinking water. *Environ. Health Perspect.* **2002**, *110*, 337–342. [CrossRef] [PubMed]
7. Magdo, H.S.; Forman, J.; Graber, N.; Newman, B.; Klein, K.; Satlin, L.; Amler, R.W.; Winston, J.A.; Landrigan, P.J. Grand rounds: Nephrotoxicity in a young child exposed to uranium from contaminated well water. *Environ. Health Perspect.* **2007**, *115*, 1237–1241. [CrossRef] [PubMed]
8. La Touche, Y.D.; Willis, D.L.; Dawydiak, O.I. Absorption and biokinetics of U in rats following an oral administration of uranyl nitrate solution. *Health Phys.* **1987**, *53*, 147–162. [CrossRef] [PubMed]
9. Paquet, F.; Houpert, P.; Blanchardon, E.; Delissen, O.; Maubert, C.; Dhieux, B.; Moreels, A.M.; Frelon, S.; Gourmelon, P. Accumulation and distribution of uranium in rats after chronic exposure by ingestion. *Health Phys.* **2006**, *90*, 139–147. [CrossRef] [PubMed]
10. Vicente-Vicente, L.; Quiros, Y.; Pérez-Barriocanal, F.; López-Novoa, J.M.; López-Hernández, F.J.; Morales, A.I. Nephrotoxicity of uranium: Pathophysiological, diagnostic and therapeutic perspectives. *Toxicol. Sci. Off. J. Soc. Toxicol.* **2010**, *118*, 324–347. [CrossRef] [PubMed]
11. United Nations Scientific Committee on the Effects of Atomic Radiation. *Sources, Effects and Risks of Ionizing Radiation: Biological Effects of Selected Internal Emitters—Uranium*; United Nations (UN): New York, NY, USA, 2016.
12. Leggett, R.W. The behavior and chemical toxicity of U in the kidney: A reassessment. *Health Phys.* **1989**, *57*, 365–383. [CrossRef] [PubMed]
13. Fujigaki, Y.; Goto, T.; Sakakima, M.; Fukasawa, H.; Miyaji, T.; Yamamoto, T.; Hishida, A. Kinetics and characterization of initially regenerating proximal tubules in S3 segment in response to various degrees of acute tubular injury. *Nephrol. Dial. Transplant. Off. Publ. Eur. Dial. Transpl. Assoc. Eur. Ren. Assoc.* **2006**, *21*, 41–50. [CrossRef] [PubMed]
14. Lu, S.; Zhao, F.Y. Nephrotoxic limit and annual limit on intake for natural U. *Health Phys.* **1990**, *58*, 619–623. [PubMed]
15. Homma-Takeda, S.; Terada, Y.; Nakata, A.; Sahoo, S.K.; Yoshida, S.; Ueno, S.; Inoue, M.; Iso, H.; Ishikawa, T.; Konishi, T.; et al. Elemental imaging of kidneys of adult rats exposed to uranium acetate. *Nucl. Instrum. Methods Phys. Res. Sect. B Beam Interact. Mater. At.* **2009**, *267*, 2167–2170. [CrossRef]
16. Homma-Takeda, S.; Kokubo, T.; Terada, Y.; Suzuki, K.; Ueno, S.; Hayao, T.; Inoue, T.; Kitahara, K.; Blyth, B.J.; Nishimura, M.; et al. Uranium dynamics and developmental sensitivity in rat kidney. *J. Appl. Toxicol.* **2013**, *33*, 685–694. [CrossRef] [PubMed]
17. Homma-Takeda, S.; Kitahara, K.; Suzuki, K.; Blyth, B.J.; Suya, N.; Konishi, T.; Terada, Y.; Shimada, Y. Cellular localization of uranium in the renal proximal tubules during acute renal uranium toxicity. *J. Appl. Toxicol.* **2015**, *35*, 1594–1600. [CrossRef] [PubMed]
18. Kitahara, K.; Numako, C.; Terada, Y.; Nitta, K.; Shimada, Y.; Homma-Takeda, S. Uranium XAFS analysis of kidney from rats exposed to uranium. *J. Synchrotron Radiat.* **2017**, *24 Pt 2*, 456–462. [CrossRef]
19. Homma-Takeda, S.; Numako, C.; Kitahara, K.; Yoshida, T.; Oikawa, M.; Terada, Y.; Kokubo, T.; Shimada, Y. Phosphorus Localization and Its Involvement in the Formation of Concentrated Uranium in the Renal Proximal Tubules of Rats Exposed to Uranyl Acetate. *Int. J. Mol. Sci.* **2019**, *20*, 4677. [CrossRef] [PubMed]
20. Takeda, M.; Hosoyamada, M.; Shirato, I.; Obinata, M.; Suzuki, M.; Endou, H. Establishment of vasopressin-responsive early proximal tubular cell lines derived from transgenic mice harboring temperature-sensitive simian virus 40 large T-antigen gene. *Biochem. Mol. Biol. Int.* **1995**, *37*, 507–515. [PubMed]
21. Takeda, M.; Kobayashi, M.; Endou, H. Establishment of a mouse clonal early proximal tubule cell line and outer medullary collecting duct cells expressing P2 purinoceptors. *Biochem. Mol. Biol. Int.* **1998**, *44*, 657–664. [CrossRef] [PubMed]
22. Hosoyamada, M.; Obinata, M.; Suzuki, M.; Endou, H. Cisplatin-induced toxicity in immortalized renal cell lines established from transgenic mice harboring temperature sensitive SV40 large T-antigen gene. *Arch. Toxicol.* **1996**, *70*, 284–292. [CrossRef]
23. Fujishiro, H.H.S. Gene expression profiles of immortalized S1, S2, and S3 cells derived from each segment of mouse kidney proximal tubules. *Fund. Toxicol. Sci.* **2019**, *6*, 117–123. [CrossRef]

24. Fujishiro, H.; Hamao, S.; Isawa, M.; Himeno, S. Segment-specific and direction-dependent transport of cadmium and manganese in immortalized S1, S2, and S3 cells derived from mouse kidney proximal tubules. *J. Toxicol. Sci.* **2019**, *44*, 611–619. [CrossRef]
25. Fujishiro, H.; Yamamoto, H.; Otera, N.; Oka, N.; Jinno, M.; Himeno, S. In Vitro Evaluation of the Effects of Cadmium on Endocytic Uptakes of Proteins into Cultured Proximal Tubule Epithelial Cells. *Toxics* **2020**, *8*, 24. [CrossRef] [PubMed]
26. Fujishiro, H.; Okugaki, S.; Kubota, K.; Fujiyama, T.; Miyataka, H.; Himeno, S. The role of ZIP8 down-regulation in cadmium-resistant metallothionein-null cells. *J. Appl. Toxicol.* **2009**, *29*, 367–373. [CrossRef]
27. Homma-Takeda, S.; Iso, H.; Ito, M.; Suzuki, K.; Harumoto, K.; Yoshitomi, T.; Ishikawa, T.; Oikawa, M.; Suya, N.; Konishi, T.; et al. Evaluation of Pressed Powders and Thin Section Standards for Multi-Elemental Analysis by Conventional and Micro-PIXE Analysis. *Int. J. PIXE* **2010**, *20*, 21–28. [CrossRef]
28. Homma-Takeda, S.; Terada, Y.; Iso, H.; Ishikawa, T.; Oikawa, M.; Konishi, T.; Imaseki, H.; Shimada, Y. Rubidium distribution in kidneys of rimmature ats. *Int. J. PIXE* **2009**, *19*, 39–45. [CrossRef]
29. Homma-Takeda, S.; Nishimura, Y.; Iso, H.; Ishikawa, T.; Imaseki, H.; Yukawa, M. A new approach for standard preparation in microbeam analysis: Development and validation. *J. Radioanal. Nucl. Chem.* **2008**, *279*, 627–631. [CrossRef]
30. Sato, C.; Sato, M.; Ogawa, S. Imaging of immunogold labeling in cells and tissues by helium ion microscopy. *Int. J. Mol. Med.* **2018**, *42*, 309–321. [CrossRef] [PubMed]
31. Roudeau, S.; Carmona, A.; Perrin, L.; Ortega, R. Correlative organelle fluorescence microscopy and synchrotron X-ray chemical element imaging in single cells. *Anal. Bioanal. Chem.* **2014**, *406*, 6979–6991. [CrossRef] [PubMed]
32. Carmona, A.; Malard, V.; Avazeri, E.; Roudeau, S.; Porcaro, F.; Paredes, E.; Vidaud, C.; Bresson, C.; Ortega, R. Uranium exposure of human dopaminergic cells results in low cytotoxicity, accumulation within sub-cytoplasmic regions, and down regulation of MAO-B. *Neurotoxicology* **2018**, *68*, 177–188. [CrossRef] [PubMed]
33. Suhard, D.; Tessier, C.; Manens, L.; Rebière, F.; Tack, K.; Agarande, M.; Guéguen, Y. Intracellular uranium distribution: Comparison of cryogenic fixation versus chemical fixation methods for SIMS analysis. *Microsc. Res. Tech.* **2018**, *81*, 855–864. [CrossRef] [PubMed]
34. Guéguen, Y.; Suhard, D.; Poisson, C.; Manens, L.; Elie, C.; Landon, G.; Bouvier-Capely, C.; Rouas, C.; Benderitter, M.; Tessier, C. Low-concentration uranium enters the HepG2 cell nucleus rapidly and induces cell stress response. *Toxicol. In Vitro Int. J. Publ. Assoc. Bibra* **2015**, *30*, 552–560. [CrossRef]
35. Ghadially, F.N.; Lalonde, J.M.; Yang-Steppuhn, S. Uraniosomes produced in cultured rabbit kidney cells by uranyl acetate. *Virchows Arch. Bcell Pathol. Incl. Mol. Pathol.* **1982**, *39*, 21–30. [CrossRef] [PubMed]
36. Mirto, H.; Henge-Napoli, M.H.; Gibert, R.; Ansoborlo, E.; Fournier, M.; Cambar, J. Intracellular behaviour of uranium(VI) on renal epithelial cell in culture (LLC-PK1): Influence of uranium speciation. *Toxicol. Lett.* **1999**, *104*, 249–256. [CrossRef]
37. Milgram, S.; Carriere, M.; Malaval, L.; Gouget, B. Cellular accumulation and distribution of uranium and lead in osteoblastic cells as a function of their speciation. *Toxicology* **2008**, *252*, 26–32. [CrossRef] [PubMed]
38. Qi, L.; Basset, C.; Averseng, O.; Quemeneur, E.; Hagege, A.; Vidaud, C. Characterization of UO2(2+) binding to osteopontin, a highly phosphorylated protein: Insights into potential mechanisms of uranyl accumulation in bones. *Met. Integr. Biometal Sci.* **2014**, *6*, 166–176. [CrossRef] [PubMed]
39. Li, B.; Raff, J.; Barkleit, A.; Bernhard, G.; Foerstendorf, H. Complexation of U(VI) with highly phosphorylated protein, phosvitin A vibrational spectroscopic approach. *J. Inorg. Biochem.* **2010**, *104*, 718–725. [CrossRef] [PubMed]
40. Pible, O.; Vidaud, C.; Plantevin, S.; Pellequer, J.L.; Quemeneur, E. Predicting the disruption by UO2(2+) of a protein-ligand interaction. *Protein Sci. Publ. Protein Soc.* **2010**, *19*, 2219–2230. [CrossRef] [PubMed]